ELSEVIER

Tectonophysics 321 (2000) 103–126

TECTONOPHYSICS

www.elsevier.com/locate/tecto

Diachronous cooling on both sides of a major strike slip fault in the Variscan Maures Massif (south-east France), as deduced from a detailed $^{40}Ar/^{39}Ar$ study

Anne-Claire Morillon [a,b], Gilbert Féraud [a,*], Marc Sosson [b], Gilles Ruffet [a], Gilbert Crevola [c], Gilles Lerouge [d]

[a] *UMR 6526 Géosciences Azur, CNRS, Université de Nice — Sophia Antipolis, Parc Valrose, 06108 Nice cedex 2, France*
[b] *UMR 6526 Géosciences Azur, CNRS, Université de Nice — Sophia Antipolis, 250 rue Albert Einstein, 06560 Valbonne, France*
[c] *Institut EGID, Université de Bordeaux III, 1 allée F. Daguin, BP 06, 33405 Talence, France*
[d] *IGAL, boulevard de L'Hautil, 95000 Cergy Pontoise, France*

Received 17 May 1999; accepted for publication 8 February 2000

Abstract

A detailed $^{40}Ar/^{39}Ar$ geochronological study was performed in the Maures Massif (SE France) to define the thermal history of this geochronologically poorly constrained segment of the Variscan belt. A total of 22 plateau ages were obtained on single grains and bulk samples of amphibole, muscovite and biotite extracted from 21 metamorphic and magmatic rocks sampled on both sides of the Grimaud Fault. Migmatites, micaschists, gneisses, pegmatites and granites displayed muscovite and biotite plateau ages ranging from 317.2 ± 1.0 to 322.9 ± 1.7 Ma on the western side and from 300.2 ± 0.6 to 306.0 ± 2.4 Ma to the east of the Grimaud fault. In the western block, amphiboles from amphibolites yielded plateau ages of 328.1 ± 2.8 and 329.9 ± 2.1 Ma, whereas in the eastern block, amphiboles from amphibolite and magmatic bodies yielded variable ages ranging from 307.9 ± 1.2 to 317.4 ± 2.4 Ma. These data clearly demonstrate distinct cooling histories between at least 330 and 300 Ma, on both sides of the Grimaud Fault, which consequently appears as a major crustal fault during the late Variscan orogeny. As shown by the concordant (for each type of mineral) data obtained on biotite, muscovite, and amphibole from magmatic and metamorphic rocks, the two crustal blocks cooled down independently, each one homogeneously, in the range of temperatures 550–300°C. Two distinct periods of fast cooling appear, at 320 Ma to the west and 305–300 Ma to the east. These data are consistent with those previously obtained on other regions of the European Variscan belt. © 2000 Elsevier Science B.V. All rights reserved.

Keywords: $^{40}Ar/^{39}Ar$; geochronology; Hercynian; Maures; Variscan

* Corresponding author. Fax: +33-4-92-07-68-16.
E-mail addresses: feraud@unice.fr (G. Féraud), sosson@faille.unice.fr (M. Sosson), crevola@egid.u-bordeaux.fr (G. Crevola), g.lerouge@tahiti.tethys-software.fr (G. Lerouge)

0040-1951/00/$ - see front matter © 2000 Elsevier Science B.V. All rights reserved.
PII: S0040-1951(00)00076-7

1. Introduction

Geochronological studies in the vicinity of major faults allow one to evaluate the thermal and kinematic parameters in different geodynamical settings.

In order to gain a better insight on the late exhumation processes involved in the Variscan belt, a detailed geochronological study was conducted on the Variscan Maures Massif (SE France). The choice of this massif was guided by the lack of precise geochronological data and the occurrence of a main fault (Grimaud Fault) (Vauchez and Bufalo, 1985, 1988) in this sector of the Variscan belt located between the 'Massifs Cristallins Externes' in the Alps, to the north-east, and the Corsica–Sardinia block, to the south.

In the Maures Massif, the Grimaud Fault represents a major discontinuity between the western and eastern metamorphic sequences. It corresponds to the western border of a steeply dipping left-lateral strike-slip shear zone that deformed migmatites of the eastern block (Vauchez and Bufalo, 1985, 1988). Precise geochronological data are necessary to evaluate (1) the thermal history on both sides of the fault, and (2) if and when these two compartments experienced distinct histories.

Previous geochronological studies on the Maures Massif mostly consist of Rb/Sr (Maluski and Allègre, 1970; Roubault et al., 1970; Maluski, 1972; Amenzou, 1988; Innocent, 1993) and U/Pb (Moussavou, 1998) measurements, and one $^{40}Ar/^{39}Ar$ study (Maluski and Gueirard, 1978). These results are either too imprecise or too scarce, or characterize too high temperature domains to determine a complete thermal history of the belt, in particular at temperatures lower than 500–550°C. Such data exist in other regions of the Variscan belt. For example, in the eastern Massif Central, structural and geochronological data document, after a crustal thickening, a decompression between 360 and 340 Ma (Costa and Rey, 1995) that was followed by thermal relaxation and post-thickening extensions along normal and transfer faults in the time interval 320–290 Ma (Caen-Vachette et al., 1982; Costa, 1990; Downes et al., 1991; Costa et al., 1993; Burg et al., 1994; Costa and Rey, 1995; Gardien et al., 1997).

This paper presents the first detailed $^{40}Ar/^{39}Ar$ study on the Maures Massif, and represents one of the most detailed geochronological studies related to a major crustal fault (the Grimaud Fault) in the belt. The investigated temperatures (on the order of 550–300°C) reflect cooling of the crust during the relaxation stage and the end of exhumation. These new data will be compared with previous geochronological results. They contribute to a better understanding of this southern part of the Variscan belt and more particularly to the processes that control exhumation of metamorphic zones.

2. Geological setting and previous geochronological data

With Corsica, the Maures Massif is the southernmost part of the Variscan internal belt in France (Fig. 1). At the end of the orogeny, exhumation of metamorphic rocks, including high-pressure relics (Le Marrec, 1976; Maquil, 1976; Caruba, 1983; Crevola et al., 1991) occurred in most parts of the massif, and two wrenching stages here related to a compressional tectonic were described (Vauchez and Bufalo, 1985, 1988).

The Maures Massif consists of two tectono-metamorphic blocks in tectonic contact along the Grimaud Fault (Bordet, 1966) and contains high-grade metamorphic rocks and intrusives, which are more numerous to the east. This N 20° E-trending sub-vertical fault is 45 km long from the coast, to the south, to the Tanneron Massif to the north (Fig. 1).

Along the western border of the Eastern Block (EB) (relative to the Grimaud Fault), a 2 km wide vertical ductile shear zone in migmatites indicates a sinistral motion during the migmatization (Vauchez and Bufalo, 1985). Schistosity planes are subvertical and stretching lineation presents a low dipping to the north or to the south (Morillon, 1997). Eastward, the metamorphic rocks are foliated and folded (occurrence of sheath fold). Stretching lineation and kinematic indicators docu-

ment a heterogeneous ductile deformation related to a top to the north sense of shear (Le Marrec, 1976; Vauchez and Bufalo, 1985; Morillon, 1997).

The EB mainly consists of migmatites composed of ortho- and para-gneisses that contain amphibolitized eclogite lenses (Le Marrec, 1976; Maquil, 1976; Caruba, 1983; Crevola et al., 1991). The *P–T* path of the EB displays a retrograde clockwise path from eclogite to amphibolite facies and anatexis (Maquil, 1976). Migmatization (at about 700°C) was dated at 325±8 Ma (on zircon, lower intercept) and 333±3 Ma (on monazite) (Moussavou and Lancelot, 1996; Moussavou, 1998).

Four distinct generations of plutons were distinguished in the EB (Crevola et al., 1991): (1) synkinematic and late migmatitic granites as the granites of Ramatuelle (Vauchez and Bufalo, 1988), Moulin-Blanc and St-Pons-les-Mures (ages unknown); (2) late- to post-kinematic granites as the peraluminous Plan-de-la-Tour granite (with megacrysts of K-feldspars, two micas and often cordierite), dated at 334±10 Ma [age recalculated with decay constants recommended by Steiger and Jäger (1977)] by the Rb/Sr method applied on whole rocks from several granitic bodies (Roubault et al., 1970), at 313±10 Ma (Rb/Sr, age recalculated, Maluski, 1972), and at 324±5 Ma on zircon (higher intercept, Moussavou, 1998); (3) post-kinematic granites as the Camarat pluton, dated at 297±5 Ma (Rb/Sr whole-rock isochron, Roubault et al., 1970, age recalculated) and 298±5 Ma (Rb/Sr, Amenzou, 1988); (4) several small late-kinematic tonalite bodies that form some kind of N–S alignment from the Grimaud area to the Tanneron Massif. At Reverdit, a tonalite body yielded a U/Pb age of 334±3 Ma on zircon (higher intercept; Moussavou, 1998). Dextral sense of shear related to intrusion stage is described in the northern part of the Plan de la Tour granite along the Grimaud Fault (Onezime et al., 1999). Several generations of pegmatite veins are late occurrences of these intrusives. Permian doleritic and rhyolitic dikes intersect the series (Zheng et al., 1991–1992).

The Western Block (WB) is composed of the three following metamorphic units (Fig. 1) (Crevola et al., 1991). The upper Western Units are composed of phyllades. The Middle Bormes Unit consists of orthogneisses dated at 344±15 Ma (on zircon, lower intercept) and 345±3 Ma (on monazite) (Moussavou and Lancelot, 1996; Moussavou, 1998), paragneisses and micaschists and some amphibolite lenses. The Lower La Garde–Freinet Unit is made of orthogneisses, amphibolites, leptynites (so-called Leptyno-Amphibolitic group), gabbros, serpentinites, garnet–spinel peridotites ($P=16$–18 kbar, $T=$ 850–860°C; Bouloton et al., 1998), and sillimanite-bearing micaschists and migmatites. The metamorphic grade increases eastward (Caruba, 1983). Recent petrographic studies suggest an earlier HP–LT stage (white schist facies) only preserved in garnet and a clockwise *P–T* path from high pressure to LP–HT (Leyreloup et al., 1996). The WB presents a main west-dipping foliation. N 90°- to N 120°-trending stretching lineation and kinematic indicators suggest a top to the WNW sense of shear (Morillon, 1997).

Minor intrusions are present in the WB. The Hermitan granite was studied by Amenzou (1988) and dated at 338±8 Ma by Moussavou (1998) (U/Pb, higher intercept).

3. Description of samples analyzed

A total of 21 samples from both sides of the Grimaud Fault were selected, according to the type of rock, the available minerals, the alteration of the rock and minerals and their spatial distribution (Fig. 1; Table 1); 15 of them were sampled along an ESE–WNW cross-section on both parts of the fault.

The Western Block: the amphibolites analyzed belong to the 'Leptyno-Amphibolitic Group' (95MO9, 93MO21). They contain hornblende, plagioclase and minor amounts of quartz and garnet. The analyzed rocks of the Bormes Unit are biotite–muscovite–garnet micaschist (93MO19), biotite micaschist (95MO6), and muscovite–biotite orthogneisses (95MO7, 95MO8, where the biotite is slightly chloritized). A biotite–sillimanite–garnet micaschist of the La Garde–Freinet Unit was also analyzed (95MO10).

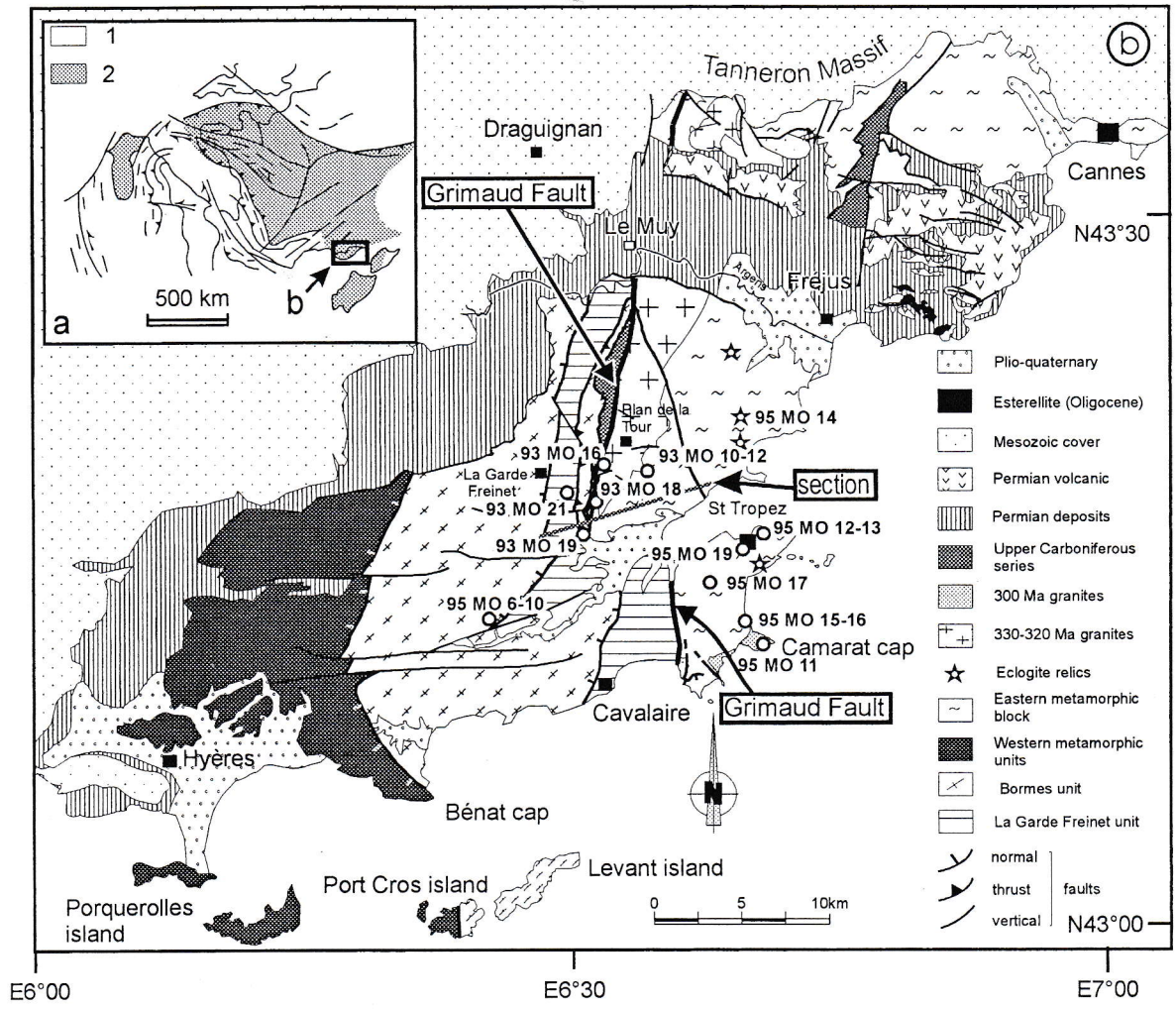
1
2
500 km
a
b
b
Tanneron Massif
Draguignan
Grimaud Fault
Le Muy
Cannes
N43°30
Frejus
Plan de la Tour
95 MO 14
93 MO 16
93 MO 10-12
La Garde Freinet
93 MO 18
93 MO 21
section
St Tropez
95 MO 12-13
93 MO 19
95 MO 19
95 MO 17
95 MO 6-10
95 MO 15-16
Camarat cap
95 MO 11
Cavalaire
Grimaud Fault
Hyères
Bénat cap
Porquerolles island
Port Cros island
Levant island
0 5 10km
Plio-quaternary
Esterellite (Oligocene)
Mesozoic cover
Permian volcanic
Permian deposits
Upper Carboniferous series
300 Ma granites
330-320 Ma granites
Eclogite relics
Eastern metamorphic block
Western metamorphic units
Bormes unit
La Garde Freinet unit
normal
thrust
vertical
faults
N43°00
E6°00
E6°30
E7°00

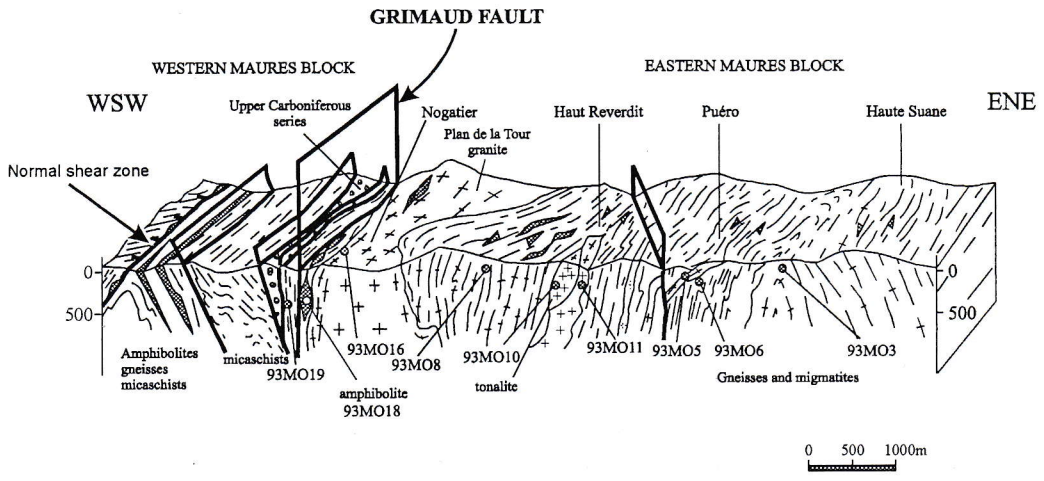
GRIMAUD FAULT
WESTERN MAURES BLOCK
EASTERN MAURES BLOCK
WSW
ENE
Upper Carboniferous series
Nogatier
Haut Reverdit
Puéro
Haute Suane
Plan de la Tour granite
Normal shear zone
0
500
Amphibolites gneisses micaschists
micaschists
93MO19
amphibolite 93MO18
93MO16
93MO8
93MO10
tonalite
93MO11
93MO5
93MO6
Gneisses and migmatites
93MO3
0 500 1000m

The Eastern Block: the metamorphic rocks analyzed are gneisses (93MO6) and migmatites (93MO3, that contain K-feldspar, plagioclase, fresh biotite and few muscovites; 93MO8, made of slightly perthitic K-feldspar, plagioclase, muscovite and biotite, and low amount of cordierite; 95MO16, containing plagioclase, few K-feldspars, and biotite affected by only scarce chloritization). The macroscopic planar anisotropy (foliation) is due to biotite-preferred orientation. The amphibolite 93MO18 was sampled in a boudin involved in the strike-slip ductile deformation related to the Grimaud Fault. This rock was affected by a ductile deformation, and consists of alternating biotite-rich and amphibole-rich layers, the first one localizing deformation. Biotite may have crystallized first, because automorphous crystals can be seen in some amphiboles. Amphibole and biotite are fresh. A second type of amphibolite, corresponding to retromorphosed eclogites (Le Marrec, 1976), has been sampled in two locations, the Bougnon pass (95MO14, containing fresh hornblende and plagioclase, and chloritized biotite) and the Bonne Terrasse Beach (95MO15, made of generally fresh green hornblende only scarcely chloritized, clinopyroxene partly included into hornblende, plagioclase transformed into sericite, opaque and titanite). These amphibolitized eclogites correspond to elongated lenses within the foliated gneisses. The second one was sampled at 20–30 m from the Camarat granite.

Among the numerous magmatic bodies of the EB, only some of them were investigated.

A tonalite (biotite–hornblende–plagioclase–quartz) (93MO10) supposed to represent an early generation hybrid magma (Amenzou, 1988), was sampled in the Reverdit quarry. Both biotite and hornblende are often strongly chloritized, but fresh grains of hornblende could be selected for analysis. Plagioclase is also strongly altered. A syntectonic leucogranite was sampled near Ste-Maxime (so-called Saint-Pons-les-Mûres two-micas granite, 93MO5). This rock is made of perthitic K-feldpar, plagioclase partially transformed at the grain periphery, and generally fresh biotite. A cordierite-rich synkinematic two-micas granite was sampled at St-Tropez (Moulin-Blanc granite, 95MO12A, containing slightly perthitic K-feldspar, plagioclase partially recrystallized at the periphery, muscovite, biotite often chloritized, abundant cordierite partly transformed in white mica).

Two distinct facies of the peraluminous porphyritic Plan-de-la-Tour granite were sampled, a non-deformed rock (93MO11, eastern edge) and a slightly foliated one (93MO16, sampled at its western edge near the Grimaud Fault, containing perthitic microcline, zoned plagioclase, fresh biotite, and scarce muscovite and cordierite).

A two-mica granite (so-called Camarat granite, 95MO11) has been sampled 20 m to the north of the Camarat lighthouse. It is considered as post-tectonic because of its E–W orientation that clearly cross-cuts the previous ductile fabrics as the foliation plane and associated stretching lineation and folds.

4. Experimental procedures

The $^{40}Ar/^{39}Ar$ analyses were performed on some bulk samples and mostly single grains of muscovite, biotite and amphibole. Grain sizes for single grain and bulk sample analyses are on the order of 400–600 μm and 160–250 μm respectively. The samples were irradiated in the nuclear reactor at McMaster University in Hamilton, Canada, in position 5c. The total neutron flux density during irradiation was 8.8×10^{18} n cm^{-2}, with a maximum flux gradient estimated at $\pm 0.2\%$ in the volume where samples were included. We used the Hb3gr hornblende as a flux monitor with an age of 1072 Ma (Turner et al., 1971). The analytical procedures for bulk sample and single grain analyses are described in detail by Féraud et al. (1982) and Ruffet et al. (1991) respectively. The gas extraction of single grains was carried out by a

Fig. 1. (a) Simplified sketch map of the Variscan units in western Europe before Golf de Gascogne opening, modified from Matte (1991): (1) external zones; (2) internal zone. (b) Structural sketch map of the Maures Massif (SE France) and location of the samples analyzed. The ESE–WNW section studied in detail is indicated in the map and a three-dimensional sketch is given below.

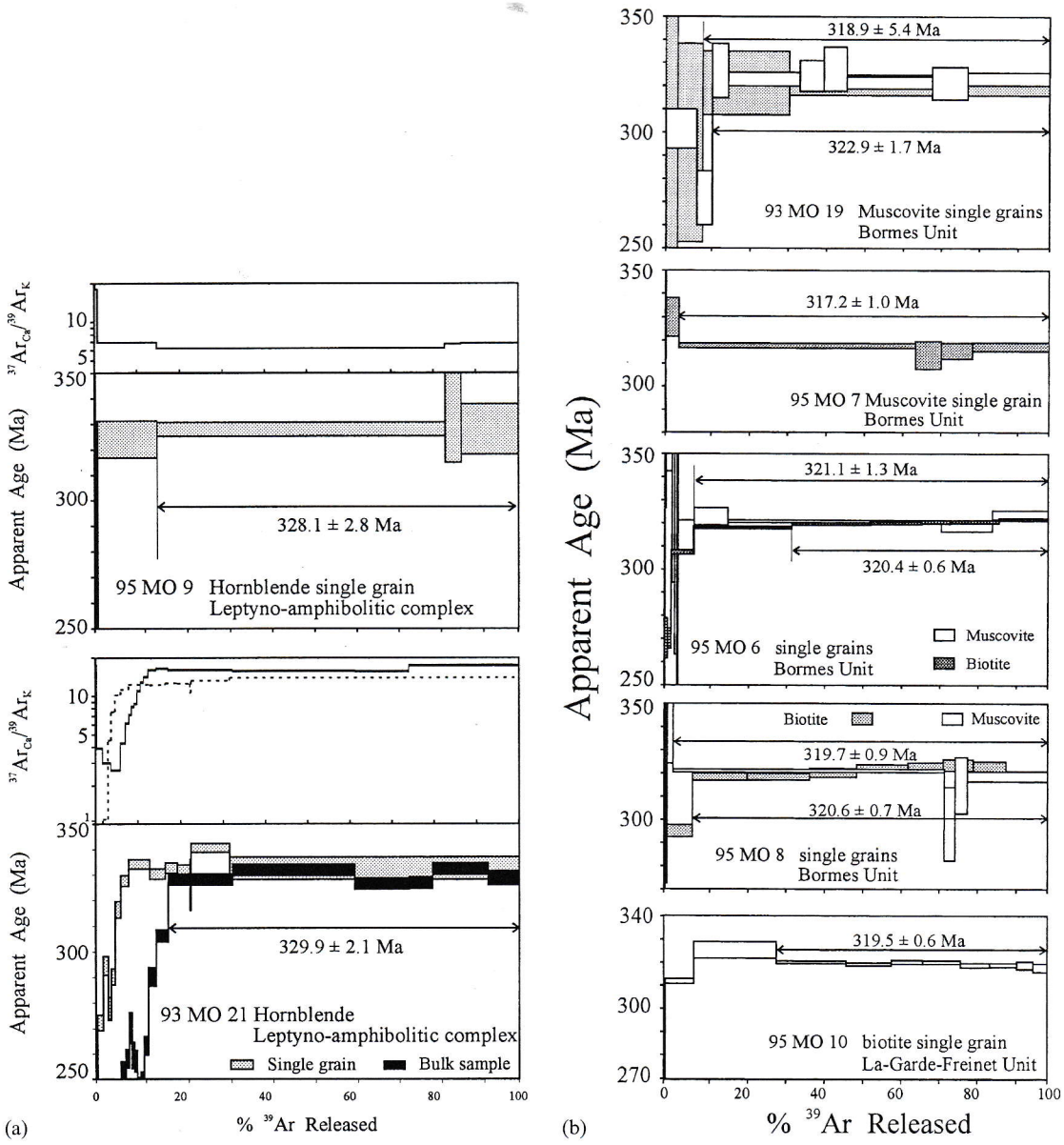

Fig. 2. (a) $^{40}Ar/^{39}Ar$ age and $^{37}Ar_{Ca}/^{39}Ar_K$ ratio spectra obtained on single grains and bulk samples of amphibole from the leptyno-amphibolitic complex, to the west of the Grimaud Fault. The error bars for apparent ages and plateau ages are indicated at the 1σ level. (b) $^{40}Ar/^{39}Ar$ age spectra obtained on single grains of muscovite and biotite from micaschists from the Bormes Unit (93MO19, 95MO6-7-8) and La Garde–Freinet Unit (95MO10) to the west of the Grimaud Fault. (c) $^{40}Ar/^{39}Ar$ age and $^{37}Ar_{Ca}/^{39}Ar_K$ ratio spectra obtained on single grains of amphibole from amphibolites (1) implicated in the sheared zone related to the Grimaud Fault (93MO18), (2) from the Col du Bougnon (95MO14) and (3) in the vicinity of the Camarat granite, at Bonne Terrasse (95MO15), all to the east of the Grimaud Fault; (*): weighted mean age, no plateau. (d) $^{40}Ar/^{39}Ar$ age spectra obtained on single grains and bulk samples of muscovite and biotite from migmatitic gneisses (93MO3A, 93MO6, 95MO16, 93MO8) and pegmatitic vein (93MO3B), to the east of the Grimaud Fault; (*): weighted mean age, no plateau. (e) $^{40}Ar/^{39}Ar$ age and $^{37}Ar_{Ca}/^{39}Ar_K$ ratio spectra obtained on single grains of amphibole, muscovite and biotite from intrusives to the east of the Grimaud Fault. Reverdit tonalite (93MO10), St Pons-les-Mûres two-micas granite (93MO5), Moulin Blanc granite (95MO12A), Plan-de-la-Tour granite (deformed: 93MO16; non-deformed: 93MO11), Camarat granite (95MO11).

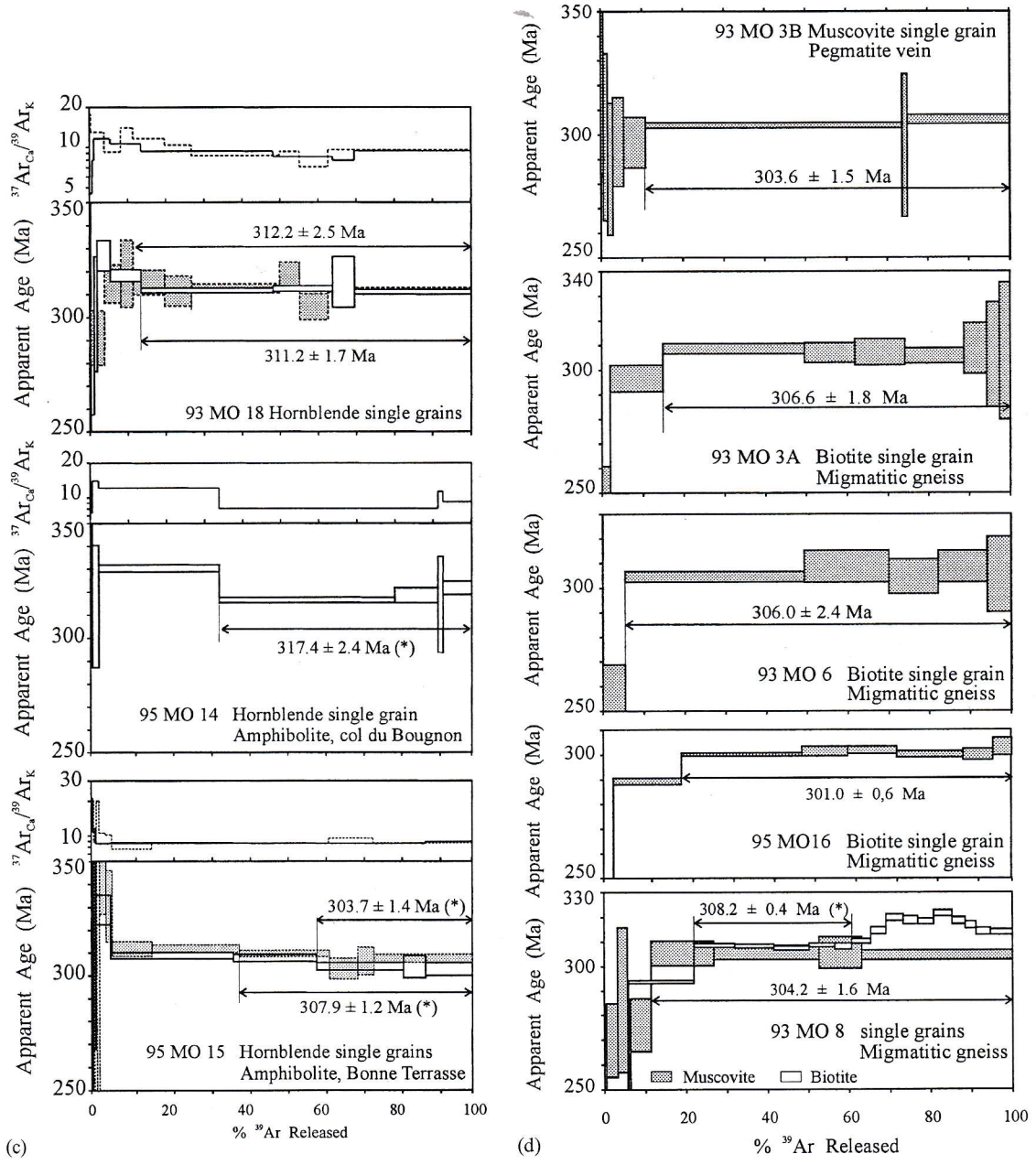

Fig. 2. (*continued*)

Coherent Innova 70-4 continuous laser and the mass spectrometer was a VG 3600 working with a Daly detector system. The typical blank values of the extraction and purification laser system were in the range 90–200, 1–4 and 2–5 $\times 10^{-14}$ cm^3 (STP) for masses 40, 39, 36 respectively, measured every third step. Correction factors for interfering isotopes produced by neutron irradiation are $(^{36}Ar/^{37}Ar)_{Ca} = 2.79 \times 10^{-4}$, $(^{39}Ar/^{37}Ar)_{Ca} = 7.06 \times 10^{-4}$ and $(^{40}Ar/^{39}Ar)_K = 3.02 \times 10^{-2}$. The criteria

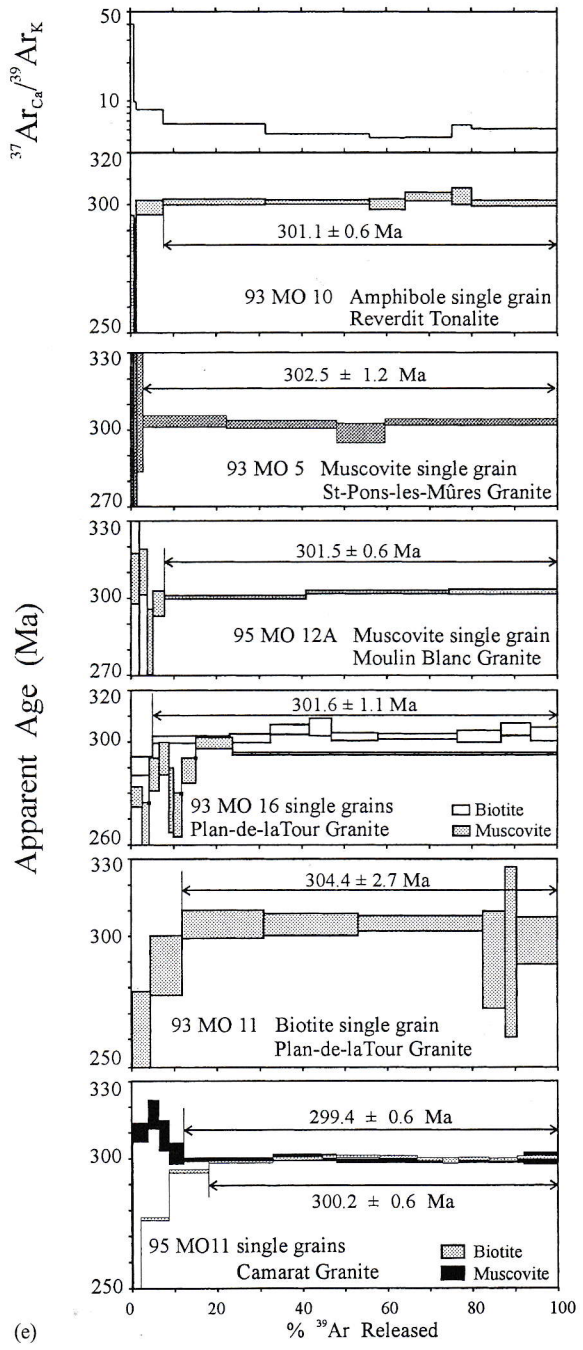

Fig. 2. (*continued*)

for defining plateau ages were the following: (1) it should contain at least 70% of released ^{39}Ar; (2) there should be at least three successive steps in the plateau; (3) the integrated age of the plateau should agree with each apparent age of the plateau within a 2σ error confidence interval. All errors are quoted at the 1σ level and do not include the errors on the age of the monitor. The error on the $^{40}Ar^*/^{39}Ar_K$ ratio of the monitor is included in the plateau age error bar calculation.

5. Results

Because of the existence of contrasted groups of ages on both sides of the fault, the data are presented separately for each block. The detailed data are presented in Table 2 in Appendix A and the plateau ages are summarized in Table 1.

5.1. Western Block

Plateau ages of 328.1 ± 2.8 and 329.9 ± 2.1 Ma were obtained on hornblende from the amphibolites 95MO9 (single grain) and 93MO21 (bulk sample) respectively (Fig. 2a). The single grain 93MO21 does not display a plateau age, but the intermediate to high temperature apparent ages are in agreement with the bulk sample plateau age. At low temperature, the single grain is less affected by alteration, as shown by the $^{37}Ar_{Ca}/^{39}Ar_K$ ratio. For the three analyses, this ratio is nearly constant on more than 80% of the spectra, demonstrating the purity of the amphibole samples analyzed.

On micaschists, gneisses and migmatites, the single grains of muscovite analyzed display four plateau ages ranging from 317.2 ± 1.0 to 322.9 ± 1.7 Ma (93MO19, 95MO6-7-8) (Fig. 2b). The biotite single grains give two plateau ages of 319.5 ± 0.6 Ma and 320.6 ± 0.7 Ma (95MO10 and 95MO8 respectively) concordant with the muscovite data, and a disturbed age spectrum (with increasing apparent ages versus temperature), probably related to scarce chloritization that was observed in thin sections (95MO6).

5.2. Eastern Block

5.2.1. Amphibolites

On the amphibolite 93MO18 (close to the Plan-de-la-Tour granite and deformed by the Grimaud

Table 1
Location, rock types and plateau ages obtained on samples from the Maures Massif. A weighted mean age is given when no plateau age could be obtained. The error bars are given at the 1σ level

Block	Unit/formation	Sample no.	Location	Rock	Mineral	Plateau age (Ma)	Weighted mean age (Ma)
West	Leptino-amphibolitic unit	95M09	La Môle quarry	amphibolite	hornblende	328.1±2.8	
		93M021	La Roche Percée (D558)	amphibolite	hornblende	329.9±2.1	
		93M019	Grimaud (D558)	garnet micaschist	muscovite	322.9±1.7	
	Bormes unit	95M07	La Môle quarry	orthogneiss	muscovite	317.2±1.0	
		95M06	La Môle quarry	biotite micaschist	muscovite	321.1±1.3	
					biotite	–	320.4±0.6
		95M08	La Môle quarry	orthogneiss	muscovite	319.7±0.9	
					biotite	320.6±0.7	
	La Garde – Freinet unit	95M010	La Môle quarry	biotite micaschist	biotite	319.5±0.6	
East	Eastern migmatite unit	93M018	West Grimaud	amphibolite	hornblende	311.2±1.7	
						312.2±2.5	
		95M014	Col de Bougnon	biotite micaschist	hornblende		317.4±2.4
		95M015	Bonne Terrassse beach	amphibolite	hornblende		307.9±1.2
							303.7±1.4
		93M03B	SE Puero	pegmatite	muscovite	303.6±1.5	
		93M03A	SE Puero	migmatitic gneiss	biotite	306.6±1.8	
		93M06	South Puero	migmatitic gneiss	biotite	306.0±2.4	
		95M016	Bonne Terrasse beach	migmatitic gneiss	biotite	301.0±0.6	
		93M08	SW Haut Reverdit	migmatitic gneiss	muscovite	304.2±1.6	
	Reverdit tonalite	93M010	Reverdit quarry	tonalite	amphibole	301.1±0.6	
	St-Pons-les-Mûres granite	93M05	Puero (GR9)	granite	muscovite	302.5±1.2	
	Moulin-Blanc granite	95M012A	Moulin Blanc school (St Tropez)	granite	muscovite	301.5±0.6	
	Plan-de-la-Tour granite	93M016	North Grimaud	granite	biotite	301.6±1.1	
		93M011	Reverdit quarry	granite	biotite	304.4±2.7	
	Camarat granite	95M011	Camarat lighthouse	granite	muscovitebiotite	299.4±0.6	
						300.2±0.6	

shear zone), two concordant plateau ages of 311.2±1.7 and 312.2±2.5 Ma are obtained on hornblende single grains (Fig. 2c). It is noticeable that these two data were obtained on two different apparatuses (line and mass spectrometers) and on samples irradiated in two distinct irradiations.

The hornblende single grain from the amphibolite 95MO14 (Col du Bougnon) displays a disturbed age spectrum characterized by higher ages at low temperature followed by lower concordant (at the 2σ level) apparent ages with a weighted mean of 317.4±2.4 Ma, representing 66.2% of ^{39}Ar released (Fig. 2c). The $^{37}Ar_{Ca}/^{39}Ar_{K}$ ratio, proportional to the Ca/K ratio, is higher at low temperature, but almost constant on the fraction corresponding to the weighted mean age (Fig. 2c). This means that this fraction of Ar released originates from a part of the grain with a homogeneous composition.

Two hornblende single grains from the amphibolite 95MO15 (Bonne Terrasse) display concordant age spectra characterized by decreasing apparent ages versus temperature, which converge towards flat segments with weighted mean ages (calculated

from three and five steps from the two experiments) of 303.7±1.4 Ma and 307.9±1.2 Ma respectively (Fig. 2c). The low-temperature steps excepted, more than 95% of the gas fraction is released by mineral phases of homogeneous composition, as shown by the constant $^{37}Ar_{Ca}/^{39}Ar_K$ ratio (Fig. 2c).

5.2.2. Migmatites

Muscovites and biotites from migmatitic gneisses (93MO3A, 93MO6, 95MO16), migmatites (93MO8) and pegmatitic veins (93MO3B) were analyzed on single grains (Fig. 2d).

The three biotite single grains from samples 93MO3A, 93MO6 and 95MO16 display plateau ages ranging from 301.0±0.6 to 306.6±1.8 Ma. The muscovite 93MO8 gives a plateau age at 304.2±1.6 Ma, whereas the biotite shows a disturbed age spectrum probably related to chloritization, as observed in thin section. The muscovite 93MO3B, from a pegmatitic vein sampled at a few centimeters from sample 93MO3A, displays a plateau age at 303.6±1.5 Ma.

5.2.3. Intrusive rocks

The muscovite single grains of the Saint-Pons-les-Mûres granodiorite (93MO5) and the Moulin-Blanc granite (95MO12A) display plateau ages at 302.5±1.2 Ma and 301.5±0.6 Ma respectively (Fig. 2e). On the Plan-de-la-Tour granite, the biotite single grain from the sample 93MO11 (undeformed) and the biotite 93MO16 (foliated, close to the amphibolite 93MO18) display plateau ages of 304.4±2.7 Ma and 301.6±1.1 Ma (concordant at the 2σ level) respectively. Despite the existence of plateau age, the second biotite shows a slightly disturbed age spectrum characteristic of the result of chloritization and ^{39}Ar recoil during the irradiation; its age is significantly higher than the single high-temperature step apparent age of 295.0± 0.5 Ma, representing 76.2% of ^{39}Ar released, displayed by the muscovite. Because of high concordance between them, the two plateau ages obtained on the biotites from two different rocks of the Plan-de-la-Tour granite are preferred to the one fusion step age given by the muscovite. On the Reverdit tonalite (93MO10), the amphibole single grain displays a plateau age of 301.1±0.6 Ma, corresponding to nearly pure amphibole, as shown by the homogeneous $^{37}Ar_{Ca}/^{39}Ar_K$ ratio representing over about 70% of the ^{39}Ar released (although thin sections show amphiboles mostly altered). The muscovite and biotite single grains from the Camarat granite (95MO11) gave concordant plateau ages of 300.2±0.6 and 299.4±0.6 Ma, the low-temperature steps excepted.

6. Discussion of data and interpretation

$^{40}Ar/^{39}Ar$ data obtained on various types of rocks and minerals, give new and precise time constraints on the late evolution of the Maures Massif. Three main aspects are discussed.

6.1. Geological significance of age data

Inside each block, and whatever the type of rock analyzed, the plateau ages are very clustered for biotite and muscovite (Fig. 3).This means that the K/Ar isotopic closure was reached at the same time at least in a large region of each block investigated. What is the geological significance of these ages? Do they result from closure by temperature decrease only or by other physical phenomena such as fluid circulation, recrystallization or deformation, or a combination of some of them? These last parameters may largely dominate in the diffusion process, but, in our case, the plateau ages (1) are homogeneous over a large region, and (2) concern different types of rock (metamorphic, magmatic) affected by no or different deformations, made of different fabrics and affected by low and different degrees of alteration. For instance, the chloritization of biotites giving similar plateau ages is variable but always low. Therefore, it is unlikely that fluid circulation, recrystallization and/or deformation, which are clearly heterogeneous in the rocks analyzed, represent the major parameters that control the isotopic exchange in the samples investigated. The measured plateau ages are more probably the result of isotopic closure mainly induced by temperature decrease; therefore, the geochronological data may

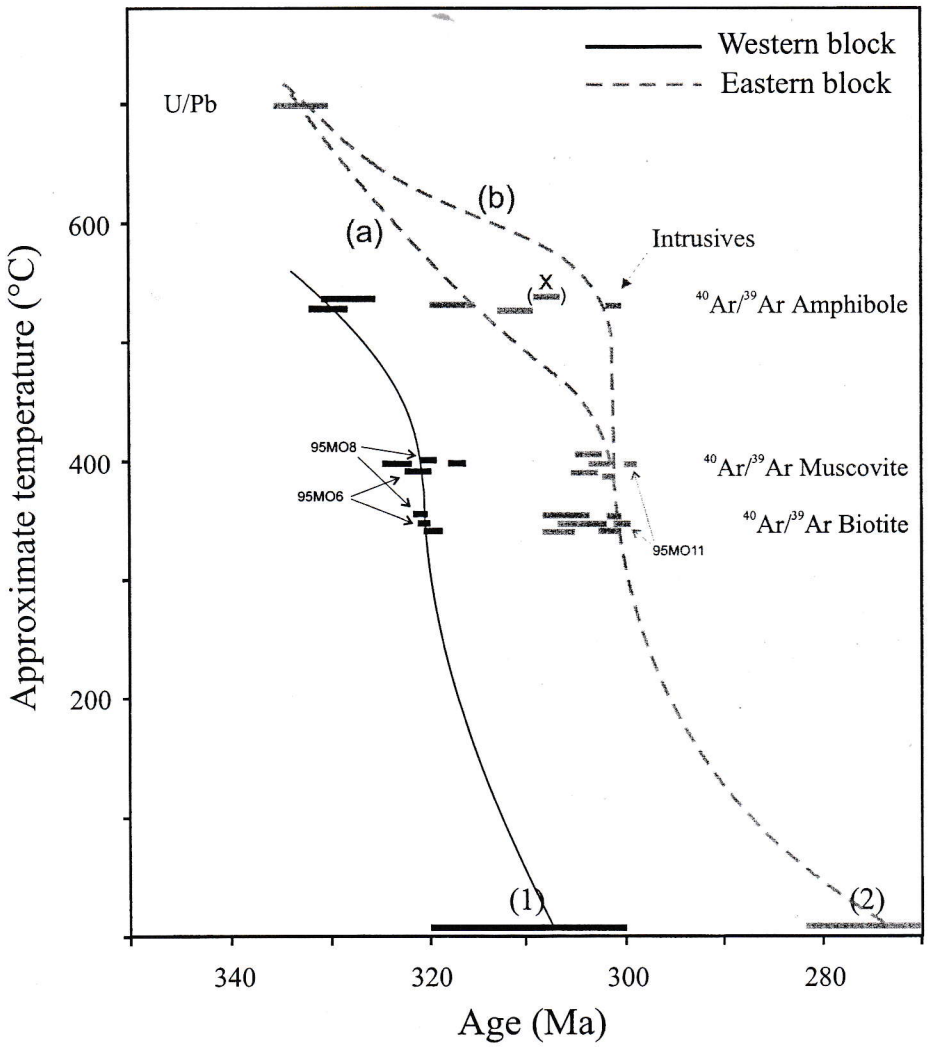

Fig. 3. Tentative temperature–time evolution for the two blocks to the east and west of the Grimaud Fault. The monazite U/Pb data concern the migmatitic gneisses from Les Cavalières (Moussavou, 1998). Because of the uncertainties on closure temperatures of the minerals investigated, the vertical temperature scale is approximate. The nearly vertical trend at 300–400°C is evidenced by precise similar plateau ages obtained on muscovite and biotite from the same rock samples (95MO6-8-11). (1) Deposition of the Stephanian basin directly on metamorphic exhumed rocks and containing erosion products of these series. (2) Deposition of the northern Permian basin containing blocks of the Plan-de-la-Tour granite, attesting to the surface exposure of the EB. (×) Plateau age on amphibole 95MO18 from a rock deformed by the Grimaud Fault. The existence of two suggested distinct paths (a) and (b) in the EB are due to ambiguous data obtained on amphiboles. Intrusives: Reverdit tonalite.

be used to reconstruct a temperature–time path for each block (Fig. 3). Nevertheless, as outlined by Villa (1998), the K/Ar closure temperature for each mineral is not yet correctly constrained, and the temperatures reported in Fig. 3 must be considered as approximate.

6.2. *The existence of two distinct blocks*

The main result of this study is the evidence of distinct ages on both sides of the Grimaud Fault. This is particularly clear for the muscovites and biotites, which display plateau ages ranging from

317.2±1.0 to 322.9±1.7 Ma on the western side (seven plateau ages) and from 300.2±0.6 to 306.0±2.4 Ma (12 plateau ages) to the east. On each side, there is no significant age difference between muscovite and biotite, which are supposed to have distinct isotopic closure temperatures.

In the EB, no age difference appears between the anatexites, the pegmatites and the plutonic rocks, suggesting that on both sides of the Grimaud Fault the whole formations cooled homogeneously and rapidly as two independent crustal blocks, in the temperature domain 300–400°C. These temperatures were reached with a time difference of about 15–20 Ma. In the EB, the thermal effects of the plutonic bodies appear negligible at that time because no age difference appears between the basement and the intrusions (the thermal equilibrium between plutons and basement was already reached).

This diachronous evolution is evidenced at higher temperature (on the order of 500–550°C) as well by the amphibole results, despite a lower quality of data. In the WB, amphiboles from two distinct samples display concordant plateau ages around 329 Ma (Fig. 2a), whereas amphiboles from the EB give younger and more variable ages. The amphibole 95MO14 displays a high-temperature weighted mean age of 317.4±2.3 Ma, whereas the amphibole 93MO18 [from an amphibolite located close to the Grimaud Fault (Fig. 2) and deformed by left-lateral motion along the shear zone] displays younger plateau ages of 311–312 Ma. The lower high-temperature ages of 304 and 308 Ma obtained on the amphibole 95MO15 could be related to the thermal influence of the Camarat granite (whole-rock Rb/Sr isochron age: 298±5 Ma; Amenzou, 1988), although the apparent distance to the granite seems too high (20–30 m) to allow significant Ar diffusion in amphibole. More data on amphibole are therefore necessary for unambiguous interpretation.

6.3. Cooling rates

These $^{40}Ar/^{39}Ar$ data, added to the U/Pb monazite age obtained on the migmatitic gneisses (Cavalières, EB; Moussavou, 1998), allow us to reconstruct a temperature–time path on the Maures Massif. The lowest temperatures are defined (1) in the WB by the Upper Carboniferous erosional surface underlying the Plan-de-la-Tour basin continental series emplaced before the brittle movement along the Grimaud Fault (Vauchez and Bufalo, 1985, 1988) and (2) in the EB by the Permian erosional surface and the deposition of the detrital sediments (conglomerates and sandstones) originated from the Plan-de-la-Tour granite (Toutin-Morin et al., 1988) [(1) and (2) respectively in Fig. 3]. Taking into account the uncertainty on the closure temperature of the minerals analyzed and the fact that the plateau ages reflect mainly closure temperatures during cooling (see above discussion), Fig. 3 shows two tentative temperature–time paths for the two blocks. The nearly vertical trends (fast cooling) around 300–400°C are constrained by very concordant and precise data obtained on both muscovite and biotite from the same rock samples (95MO6 and 95MO8 in the WB, 95MO11 in the EB, shown in Fig. 3). This fast cooling occurred at 320 Ma in the WB and at 300–305 Ma in the EB.

Cooling rates are less constrained at temperatures higher than 400°C, because of the less numerous and more ambiguous results obtained on amphiboles, particularly in the EB. The youngest age of 301.1 Ma measured on the tonalite (93MO10) is much younger than both the U/Pb age of 334±3 Ma (high intercept; Moussavou, 1998) measured on the tonalite itself, and the U/Pb age of 324±5 Ma (high intercept) measured on the Plan-de-la-Tour granite (Moussavou, 1998). Therefore, the tonalite $^{40}Ar/^{39}Ar$ age cannot represent the initial cooling of the tonalite body itself, but could reflect the cooling of the whole area. Nevertheless, in that case, it strongly disagrees with the data obtained on amphibolites from the EB. Because of the inconsistency of these data, more measurements on amphibole (in progress) are necessary.

The Stephanian deposits (Basso, 1985) unconformably cover the micaschists and gneisses of the eastern border of the WB. Consequently, our results are consistent with the 320 Ma late exhumation uplift and active erosion of the non-metamor-

phic cover of the WB before the Stephanian. For the EB, at the same time (330–320 Ma), thermochronological constraints are consistent with the high-temperature deformation along the sinistral shear zone of the gneisses, migmatites and western border of Plan-de-la-Tour granite (Vauchez and Bufalo, 1985, 1988; Morillon, 1997). Between 320 and 300 Ma, cooling occurred with a probable increasing rate in the range 305–300 Ma (Fig. 3). The high cooling rate at this time and the 280 Ma (Lower Permian) erosional surface of the EB documented that the uplift related to the end of the exhumation acted in the 300–280 Ma time interval. Consequently, we can assume that the ductile to brittle transition along the Grimauld Fault was spanned during this range of time. As the Grimaud Fault is overlain to the north by the Permian detrital deposits, brittle structures as sub-horizontal slickensides on the fault plane (Vauchez and Bufalo, 1988; Morillon, 1997) are related to the 300–280 Ma cooling event.

6.4. *Role of the Grimaud Fault on cooling evolution*

Concerning the role of the Grimaud Fault during cooling, the 15 to 20 Ma diachronous ages of cooling events recorded within the metamorphic and plutonic rocks of the Maures Massif suggest the following two hypotheses. (1) The EB corresponds to deeper crustal units than those of the WB, and exhumation succeeded to the unroofing of western units 15 to 20 Ma later, without major lateral motion between the two blocks during and after the cooling periods. In this case, the biotites and muscovites investigated from rocks of the WB located near the contact with the EB would be affected by a thermal effect induced by the exhumation of hot EB at 305–300 Ma, which is not observed in our data. Moreover, the Grimaud Fault would play as a detachment fault with a major normal throw. However, no evidence of normal component documented by west-dipping schistosity plane, down dip lineation, and top to the NW shear sense occurs close to the fault and in its presumed footwall (Vauchez and Bufalo, 1988; Morillon, 1997). (2) Both blocks were distant from each other during the evidenced cooling periods and represent distinct regions in the Hercynian belt. They came in contact along the Grimaud Fault at the end of the EB uplift, at 300–280 Ma. This seems more in agreement with our data, and the interpretation based on structural analysis of Vauchez and Bufalo (1985, 1988). This would be similar to the modern view on the Hercynian evolution of the Ivrea and Strona zones, where two distinct retrograde paths along a vertical fault are documented (Boriani and Villa, 1997). However, in this case, the lateral motion along the Grimaud Fault cannot explain the EB exhumation. A more realistic view is that the fault must have played as a transfer fault zone merged with a possible E–W-trending detachment fault. Nevertheless, such E–W-trending detachment is unknown in the Maures and Tanneron massifs. The top to the north sense of shear described by Vauchez and Bufalo (1988) and the left-lateral ductile deformation along the Grimaud Fault in the EB could be related to EB doming and its exhumation conducted by a south-dipping detachment fault that could be presently located south of the massif within north Ligurian margin tilted blocks as suggested by Rollet (1999) (Fig. 1).

7. Conclusions

(1) Metamorphic and magmatic rocks from both sides of the Grimaud Fault display 22 plateau ages. The muscovites and biotites from migmatites, micaschists, gneisses, pegmatites and granites give plateau ages ranging from 317.2 ± 1.0 to 322.9 ± 1.7 Ma on the western side (seven plateau ages) and from 300.2 ± 0.6 to 306.0 ± 2.4 Ma (12 plateau ages) to the east. To the west, amphiboles display plateau ages of 328.1 ± 2.8 and 329.9 ± 2.1 Ma. In the EB, amphiboles from amphibolites and a tonalite display ages ranging from 301 to 317 Ma.

(2) These data show distinct cooling histories from at least 330 Ma on both sides of the Grimaud Fault, which confirm that this fault was a major crustal fault during the late evolution of the southern Variscan belt. In the two blocks, the same temperatures were reached with a time interval of 15–20 Ma.

(3) For each block, there is no significant age difference for the same minerals from different rocks. Therefore, on both sides of the Grimaud Fault, the blocks cooled down homogeneously as two independent crustal blocks, in a temperature range of about 550–300°C. In the EB, the plutonic bodies investigated were in thermal equilibrium with the basement at that time and in the temperature interval 300–400°C, because no age difference appears between the basement and the intrusives.

(4) Fast cooling probably occurred in each block, at 320 Ma in the WB, and at 305–300 Ma in the EB.

(5) In the WB, the 330 to 320 Ma deformation corresponds to a probable late exhumation related to a collapse stage conducted by a normal WNW shear sense within the belt. During the same time interval, the EB was in depth evolving along an NE–SW transfer vertical ductile shear zone associated with melting of the crust. In the 305–300 Ma time interval, active erosion occurred at the surface and continental fluvial deposits covered the previously exhumed western metamorphic rocks. To the east, uplift occurred and the migmatitic rocks were deformed in ductile to brittle condition along the Grimaud Fault. The Plan-de-la-Tour granite is eroded and is a source of continental deposit toward the north since 280 Ma at least (age of the Permian deposits overlying the granite).

(6) The Carboniferous cooling evolution of the Maures Massif evidenced by our data is in general agreement with those previously obtained in other regions of the European Variscan Belt, as for example the eastern (Costa et al., 1993) and western (Bouchot et al., 1999) Massif Central or the Bohemian massif (Matte et al., 1990). During the late exhumation events, wrenching between 320 and 300 Ma is supposed to be associated with two orthogonal stages of extension (Faure, 1995) and/or occurrence of a transfer fault zone (Burg et al., 1990, 1994). Our data suggest that the late exhumation of the Maures Massif was guided by a combination of normal and transfer faults zones along which Upper Carboniferous intramountain basins unconformably overlie the first exhumed rocks.

Acknowledgements

This work has received financial support from BRGM/SGN to perform new structural and geochronological studies for the French geological mapping project (1/50 000ème St Tropez–Cap Lardier). Géosciences Azur contribution no. 315.

Appendix A

Table 1
Detailed $^{40}Ar/^{39}Ar$ analytical results. $^{40}Ar^*$ = radiogenic ^{40}Ar; Ca and K: produced by Ca and K neutron interference, respectively. Error bars are given at the 1σ level

Steps	Atmospheric contamination (%)	$\%^{39}Ar$	$^{37}Ar_{Ca}/^{39}Ar_K$	$^{40}Ar^*/^{39}Ar_K$	Age $\pm 1\sigma$ (Ma)
95MO9	*Amphibole*		*Single grain*		
1	99.57	0.24	45.700	1.89 ± 18.21	55.4 ± 526.5
2	100.0	0.48	17.200	–	–
3	10.49	13.98	7.0200	11.90 ± 0.29	324.1 ± 7.3
4	0.75	68.07	6.4600	12.06 ± 0.11	327.9 ± 2.7
5	–	3.79	7.4700	12.81 ± 1.28	346.4 ± 31.5
6	3.174	13.44	7.4400	12.06 ± 0.40	328.0 ± 9.9
Integrated age:					326.0 ± 19.8
93MO21	*Amphibole*		*Single grain*		
1	79.51	0.44	0.924	4.608 ± 0.21	243.3 ± 10.4
2	56.08	1.32	0.473	5.197 ± 0.06	272.2 ± 3.0
3	47.29	1.19	1.090	5.658 ± 0.08	294.4 ± 3.7
4	24.42	0.74	4.520	5.310 ± 0.09	277.7 ± 4.4
5	20.39	0.88	7.550	5.570 ± 0.07	290.2 ± 3.2
6	14.93	1.28	10.200	6.117 ± 0.07	316.4 ± 3.3
7	8.60	1.95	11.200	6.354 ± 0.04	327.6 ± 2.1
8	9.53	4.92	12.300	6.494 ± 0.04	334.1 ± 1.8
9	9.94	3.60	12.200	6.411 ± 0.04	330.3 ± 2.0
10	7.47	2.83	12.600	6.464 ± 0.04	332.7 ± 2.0
11	10.12	2.99	12.500	6.441 ± 0.05	331.7 ± 2.2
12	8.20	0.29	10.600	6.321 ± 0.21	326.0 ± 9.9
13	10.85	9.00	13.200	6.631 ± 0.04	340.6 ± 1.8
14	6.26	68.56	13.900	6.461 ± 0.09	332.6 ± 4.4
Integrated age:					330.6 ± 8.9
93MO21	*Amphibole*		*Bulk sample*		
1	98.2	0.29	17.30	2.93 ± 1.42	158.2 ± 52.7
2	72.81	1.33	3.8	3.65 ± 0.14	195.2 ± 4.5
3	80.11	1.97	2.98	4.24 ± 0.28	224.9 ± 8.5
4	86.58	2.22	2.61	3.01 ± 0.19	162 ± 7.3
5	58.36	1.25	4.27	4.82 ± 0.10	253.6 ± 3.1
6	58.37	0.78	6.10	4.90 ± 0.13	257.8 ± 3.6
7	55.09	0.68	7.09	5.15 ± 0.24	270.1 ± 6.1
8	57.16	0.57	8.24	4.93 ± 0.20	259.2 ± 5.1
9	57.02	0.68	8.69	4.88 ± 0.16	256.8 ± 4.2
10	60.59	0.79	10.90	4.63 ± 0.22	244.4 ± 6.0
11	63.21	0.80	12.70	4.67 ± 0.22	246.6 ± 6.0
12	56.63	1.03	14.00	5.00 ± 0.11	262.8 ± 3.7
13	40.56	1.86	15.80	5.56 ± 0.12	289.9 ± 3.7
14	26.91	2.84	16.30	5.89 ± 0.05	305.8 ± 2.3
15	13.42	15.10	16.00	6.36 ± 0.05	327.9 ± 2.1
16	9.22	28.90	15.60	6.44 ± 0.05	331.6 ± 2.2
17	11.02	12.93	25.60	6.33 ± 0.05	326.3 ± 2.2
18	17.62	5.58	17.20	6.33 ± 0.05	326.6 ± 2.4
19	14.78	13.04	17.20	6.45 ± 0.05	331.9 ± 2.3
20	31.63	7.36	17.20	6.37 ± 0.07	328.4 ± 2.8
Integrated age:					315.6 ± 5.6

Appendix A (*continued*)

Steps	Atmospheric contamination (%)	$\%^{39}Ar$	$^{37}Ar_{Ca}/^{39}Ar_K$	$^{40}Ar^*/^{39}Ar_K$	Age $\pm 1\sigma$ (Ma)
93MO19	*Muscovite (1)*		*Single grain*		
1	68.22	0.045	4.1722	4.6346 ± 34.15	244.7 ± 168.5
2	13.98	3.005	0.384 56	6.6492 ± 2.06	341.4 ± 96.3
3	12.07	6.421	0.085 15	5.6789 ± 0.89	295.5 ± 42.8
4	–	22.7	0.027 28	6.2209 ± 0.29	321.3 ± 13.8
5	–	67.82	0.003 46	6.1991 ± 0.09	320.3 ± 4.4
Integrated age:					319.5 ± 5.9
93MO19	*Muscovite (2)*		*Single grain*		
1	100.0	0.125	77.7	–	–
2	15.78	7.92	1.93	5.609	301.7 ± 8.5
3	18.32	3.92	1.47	5.191	271.9 ± 11.6
4	–	4.15	0	6.333 ± 0.25	326.6 ± 11.7
5	–	18.84	0	6.254 ± 0.06	322.9 ± 2.9
6	–	6.17	0.541	6.287 ± 0.14	324.4 ± 6.7
7	0.88	5.97	0	6.348 ± 0.20	327.3 ± 9.5
8	–	22.29	0	6.221 ± 0.05	321.3 ± 2.5
9	–	9.40	0	3.218 ± 0.15	321.1 ± 7.0
10	–	21.20	0	6.256 ± 0.06	322.9 ± 2.7
Integrated age:					318.9 ± 5.4
95MO7	*Muscovite*		*Single grain*		
1	68.19	0.19	–	7.541 ± 6.70	212.3 ± 178.1
2	11.66	3.33	0.001	12.116 ± 0.33	329.9 ± 8.3
3	3.53	61.61	–	11.628 ± 0.05	317.8 ± 1.1
4	2.18	6.74	0.009	11.462 ± 0.24	313.6 ± 6.1
5	3.41	8.26	0.016	11.537 ± 0.14	315.5 ± 3.4
6	1.24	19.87	0.005	11.605 ± 0.08	317.2 ± 1.9
Integrated age:					317.4 ± 1.0
95MO6	*Muscovite*		*Single grain*		
1	–	0.008	0.001 99	33.351 ± 150.02	792.1 ± 2883.8
2	93.84	0.100	0	1.103 ± 10.24	32.6 ± 299.9
3	–	0.039	0	10.789 ± 31.81	2.96 ± 804.9
4	–	0.248	0.891	16.271 ± 4.39	429.7 ± 103.1
5	3.75	1.540	0	13.651 ± 1.01	367.1 ± 24.5
6	4.04	0.647	0	12.235 ± 1.53	332.3 ± 37.9
7	35.30	0.593	0	11.709 ± 2.34	319.2 ± 55.9
8	26.63	0.328	0	11.365 ± 3.95	310.6 ± 99.1
9	5.31	4.138	0.0441	11.497 ± 0.29	313.9 ± 7.4
10	–	8.676	0.0152	11.861 ± 0.15	322.9 ± 3.7
11	0.25	55.874	0.004 13	11.775 ± 0.03	320.8 ± 0.6
12	1.58	13.304	0.003 84	11.673 ± 0.07	318.3 ± 1.8
13	–	14.505	0	11.888 ± 0.07	323.6 ± 1.8
Integrated age:					321.6 ± 1.1

Appendix A (*continued*)

Steps	Atmospheric contamination (%)	$\%^{39}Ar$	$^{37}Ar_{Ca}/^{39}Ar_K$	$^{40}Ar^*/^{39}Ar_K$	Age $\pm 1\sigma$ (Ma)
95MO6	*Biotite*		*Single grain*		
1	62.76	0.77	0	9.780 ± 0.34	270.3 ± 8.7
2	29.41	0.91	0.0324	9.774 ± 0.17	270.2 ± 4.4
3	3.54	5.71	0.00151	11.244 ± 0.03	307.5 ± 0.8
4	1.26	25.69	0.002 19	11.670 ± 0.02	318.2 ± 0.5
5	0.68	10.36	0.0033	11.728 ± 0.02	319.7 ± 0.5
6	1.02	13.50	0.006 07	11.475 ± 0.02	320.1 ± 0.6
7	0.87	7.75	0.008 74	11.766 ± 0.03	320.6 ± 0.8
8	0.82	12.47	0.0101	11.768 ± 0.03	320.7 ± 0.6
9	0.74	12.82	0.0101	11.808 ± 0.02	321.7 ± 0.6
Integrated age:					318.3 ± 0.2
95MO8	*Muscovite*		*Single grain*		
1	100	0.0028	0.651	–	–
2	–	0.13	0	11.767 ± 11.75	321 ± 293.7
3	–	0.17	0.156	13.904 ± 9.14	373.2 ± 293.7
4	–	0.54	0	13.809 ± 4.07	371.6 ± 99.0
5	–	1.44	0.0204	12.947 ± 1.07	350.5 ± 26.3
6	0.54	70.85	0	11.761 ± 0.03	321.1 ± 0.7
7	7.18	2.81	0	10.858 ± 0.63	298.4 ± 15.8
8	2.5	3.22	0	11.512 ± 0.48	314.9 ± 12.1
9	0.10	20.83	0	11.663 ± 0.08	318.6 ± 2.1
Integrated age:					320.6 ± 1.3
95MO8	*Biotite*		*Single grain*		
1	73.29	0.307	0.196	5.245 ± 1.97	150.3 ± 54.1
2	9.77	7.79	0.0139	10.735 ± 0.11	295.2 ± 2.7
3	1.35	14.16	0.004 57	11.657 ± 0.06	318.5 ± 1.6
4	1.33	16.40	0.003 01	11.600 ± 0.06	318.6 ± 1.4
5	1.58	12.19	0.003 86	11.727 ± 0.08	320.2 ± 1.9
6	0.91	13.42	0.003 55	11.803 ± 0.07	322.1 ± 1.7
7	0.71	9.28	0.006 66	11.823 ± 0.08	322.6 ± 2.0
8	0.89	7.81	0.007 65	11.859 ± 0.10	323.5 ± 2.4
9	0.74	8.55	0.0115	11.828 ± 0.09	322.8 ± 2.2
10	0.53	10.81	0.005 46	11.677 ± 0.07	319.0 ± 1.8
Integrated age:					318.3 ± 0.6
95MO10	*Biotite*		*Single grain*		
1	54.30	0.41	0.0881	9.158 ± 0.35	254.3 ± 9.1
2	10.83	7.36	0.007 32	11.416 ± 0.04	311.8 ± 1.1
3	–	21.48	–	11.963 ± 0.14	325.5 ± 3.6
4	0.68	18.22	0.003 48	11.749 ± 0.02	320.2 ± 0.6
5	1.75	11.79	0.004 50	11.711 ± 0.02	319.2 ± 0.6
6	0.48	8.34	0.005 64	11.748 ± 0.03	320.2 ± 0.8
7	0.51	9.83	0.0286	11.744 ± 0.03	320.1 ± 0.7
8	0.78	7.53	0.0111	11.693 ± 0.04	318.6 ± 0.9
9	0.79	7.11	0.0173	11.696 ± 0.03	318.9 ± 0.8
10	0.89	4.21	0.0231	11.694 ± 0.07	318.8 ± 1.7
11	1.17	3.71	0.0176	11.654 ± 0.07	317.8 ± 1.8
Integrated age:					320.0 ± 0.8

Appendix A (*continued*)

Steps	Atmospheric contamination (%)	$\%^{39}Ar$	$^{37}Ar_{Ca}/^{39}Ar_K$	$^{40}Ar^*/^{39}Ar_K$	Age $\pm 1\sigma$ (Ma)
93MO18	*Amphibole (1)*		*Single grain*		
1	99.64	0.28	15.4	1.5987 ± 7.33	88.2 ± 384
2	59.66	0.64	11.8	5.1052 ± 0.49	267.7 ± 23.1
3	18.63	4.27	7.99	6.1102 ± 0.35	316.1 ± 17.7
4	2.09	3.19	13.0	6.5617 ± 0.62	337.3 ± 29.0
5	5.71	8.29	10.4	6.2392 ± 0.23	322.2 ± 10.9
6	2.47	7.00	9.16	6.1229 ± 0.27	316.6 ± 12.9
7	6.64	23.27	7.35	6.0316 ± 0.08	312.3 ± 4.0
8	–	5.24	8.03	6.2747 ± 0.25	323.8 ± 12.2
9	10.43	7.42	5.93	5.7072 ± 0.24	296.8 ± 11.5
10	11.78	37.38	8.25	5.9931 ± 0.05	310.5 ± 2.3
Integrated age:					311.0 ± 2.7
93MO18	*Amphibole (2)*		*Single grain*		
1	94.10	0.72	3.49	12.4822 ± 2.69	675.1 ± 104.7
2	86.12	0.44	7.26	2.2876 ± 1.59	124.9 ± 34.0
3	60.70	0.83	10.6	5.6692 ± 1.06	295.0 ± 51.0
4	50.16	3.43	10.6	6.6689 ± 0.28	342.4 ± 13.2
5	21.41	8.00	9.51	6.2902 ± 0.11	324.6 ± 5.3
6	19.39	34.79	8.21	6.0075 ± 0.04	311.2 ± 2.0
7	2.85	15.53	7.32	6.0355 ± 0.06	313.5 ± 2.7
8	5.31	5.81	6.76	6.0971 ± 0.37	315.4 ± 17.6
9	16.58	30.45	8.21	5.9775 ± 0.04	309.7 ± 2.1
Integrated age:					315.3 ± 1.9
95MO14	*Amphibole*		*Single grain*		
1	66.89	0.31	7.88	43.0576 ± 4.21	969.8 ± 74.9
2	74.05	0.25	7.41	15.1166 ± 3.78	402.5 ± 96.1
3	18.08	1.63	14.1	11.4939 ± 0.86	313.9 ± 26.6
4	5.91	31.60	12.2	12.1523 ± 0.06	330.3 ± 1.5
5	3.12	46.17	8.07	11.5981 ± 0.05	316.5 ± 1.2
6	3.31	11.36	8.07	11.6790 ± 0.13	318.5 ± 3.3
7	8.54	1.28	11.3	11.5160 ± 0.82	314.4 ± 20.9
8	4.25	7.42	9.2	11.8063 ± 0.12	321.7 ± 2.9
Integrated age:					324.0 ± 1.1
95MO15	*Amphibole (1)*		*Single grain*		
1	97.91	0.36	21.5	14.3347 ± 5.77	384.3 ± 137.9
2	70.27	0.17	10.9	34.1535 ± 14.25	808.8 ± 270.4
3	75.01	0.67	11.7	11.7437 ± 2.06	320.6 ± 52.6
4	18.99	3.85	8.65	12.0702 ± 0.27	328.8 ± 6.5
5	7.01	32.29	8.72	11.2703 ± 0.06	308.8 ± 1.4
6	1.54	21.94	8.69	11.2294 ± 0.06	307.7 ± 1.5
7	2.73	22.79	8.62	11.0850 ± 0.06	304.1 ± 1.6
8	2.71	5.81	8.66	11.0764 ± 0.17	303.9 ± 4.8
9	8.49	12.12	8.97	11.0351 ± 0.10	302.8 ± 2.8
Integrated age:					308.6 ± 1.2

Appendix A (*continued*)

Steps	Atmospheric contamination (%)	$\%^{39}Ar$	$^{37}Ar_{Ca}/^{39}Ar_K$	$^{40}Ar^*/^{39}Ar_K$	Age $\pm 1\sigma$ (Ma)
95MO15	*Amphibole (2)*		*Single grain*		
1	86.31	0.88	20.8	10.2534 ± 2.04	282.9 ± 52.25
2	27.02	0.64	9.02	18.8497 ± 1.87	490.2 ± 42.5
3	74.49	0.69	20.5	8.4883 ± 1.67	237.2 ± 43.7
4	11.80	1.67	10.8	12.5737 ± 0.57	341.3 ± 14.2
5	–	1.65	10.4	12.1419 ± 0.63	330.6 ± 15.6
6	7.51	10.50	7.79	11.3944 ± 0.13	311.9 ± 3.2
7	2.46	22.84	8.74	11.3966 ± 0.07	322.9 ± 1.6
8	1.38	23.68	8.76	11.3156 ± 0.05	309.9 ± 1.4
9	3.68	7.49	9.65	11.0502 ± 0.18	303.2 ± 4.7
10	4.84	4.21	9.72	11.1834 ± 0.26	306.6 ± 6.1
11	5.87	25.72	8.85	11.2286 ± 0.07	307.7 ± 1.8
Integrated age:					310.7 ± 1.1
93MO3B	*Muscovite*		*Single grain*		
1	3.59	0.54	–	6.6939 ± 1.28	343.5 ± 59.7
2	9.21	1.03	–	5.7534 ± 0.71	299.1 ± 33.9
3	22.84	1.32	–	5.4803 ± 0.56	285.9 ± 26.8
4	8.05	2.65	0.014 29	5.7122 ± 0.37	297.1 ± 17.9
5	6.29	5.32	0.005 45	5.7082 ± 0.21	296.9 ± 10.3
6	0.78	62.85	0.001 52	5.8516 ± 0.02	303.7 ± 1.1
7	3.29	1.33	–	5.6785 ± 0.60	295.5 ± 28.9
8	0.11	24.95	0.000 92	5.9015 ± 0.04	306.1 ± 1.3
Integrated age:					303.6 ± 1.3
93MO3A	*Biotite*		*Single grain*		
1	55.79	1.99	0.019 67	4.1409 ± 0.81	220.1 ± 40.6
2	2.73	12.94	0.006 95	5.7022 ± 0.11	296.6 ± 5.4
3	0.06	34.62	0.001 46	5.9562 ± 0.04	308.7 ± 2.1
4	1.07	12.38	0.000 82	5.9199 ± 0.08	306.9 ± 4.0
5	0.92	12.32	0.001 41	5.937 ± 0.11	307.3 ± 5.3
6	1.09	14.46	0.000 08	5.8939 ± 0.06	305.7 ± 3.1
7	–	5.49	–	5.9561 ± 0.22	308.7 ± 10.4
8	0.64	3.13	0.01281	5.9035 ± 0.45	306.2 ± 21.3
9	–	2.66	0.002 778	5.9327 ± 0.58	307.6 ± 27.8
Integrated age:					304.5 ± 1.9
93MO6	*Biotite*		*Single grain*		
1	23.39	5.39	0.000 01	4.7363 ± 0.40	249.7 ± 19.7
2	0.40	43.96	–	5.8848 ± 0.05	305.3 ± 2.2
3	–	20.7	–	5.9719 ± 0.14	309.5 ± 6.5
4	2.33	12.17	–	5.8844 ± 0.15	305.3 ± 7.0
5	1.52	11.94	0.0017	5.9697 ± 0.14	309.4 ± 6.4
6	0.92	5.82	–	5.9020 ± 0.32	306.1 ± 15.3
Integrated age:					303.7 ± 2.4

Appendix A (*continued*)

Steps	Atmospheric contamination (%)	$\%^{39}Ar$	$^{37}Ar_{Ca}/^{39}Ar_K$	$^{40}Ar^*/^{39}Ar_K$	Age $\pm 1\sigma$ (Ma)
95MO16	*Biotite*		*Single grain*		
1	75.46	2.22	0.0683	7.155 ± 0.36	201.6 ± 9.5
2	8.38	16.69	0.0142	10.531 ± 0.05	289.5 ± 1.3
3	1.97	29.65	0.0103	10.958 ± 0.03	300.3 ± 0.7
4	1.30	11.24	0.000 000 83	11.012 ± 0.08	301.7 ± 1.9
5	1.79	12.02	0.000 000 776	11.031 ± 0.06	302.2 ± 1.5
6	2.18	16.33	0.005 76	10.963 ± 0.05	300.5 ± 1.3
7	2.05	7.22	0.001 30	10.962 ± 0.09	300.4 ± 2.3
8	1.36	4.62	0.000 002 03	11.082 ± 0.143	303.4 ± 3.6
Integrated age:					296.9 ± 0.6
93MO8	*Biotite*		*Single grain*		
1	44.58	1.46	0.354	4.499 ± 0.11	234.3 ± 5.1
2	8.64	4.38	0.208	3.989 ± 0.03	208.4 ± 1.6
3	1.41	16.08	0.005 41	5.691 ± 0.01	291.3 ± 0.6
4	0.84	9.96	0.000 002 45	5.998 ± 0.02	305.5 ± 0.8
5	0.64	9.61	0.000 002 54	5.993 ± 0.02	304.6 ± 0.7
6	0.66	8.73	0.0636	4.979 ± 0.02	304.6 ± 0.8
7	0.34	6.25	0.000 003 96	6.001 ± 0.02	305.7 ± 0.8
8	0.77	4.10	0.0466	5.993 ± 0.03	305.3 ± 1.2
9	0.71	4.77	0.0211	6.037 ± 0.02	307.4 ± 0.9
10	0.52	3.74	0.125	6.130 ± 0.03	311.7 ± 1.4
11	0.35	4.24	0.124	6.242 ± 0.03	316.9 ± 1.2
12	0.87	3.61	0.148	6.222 ± 0.03	315.9 ± 1.5
13	1.55	3.84	0.149	6.211 ± 0.02	315.5 ± 1.1
14	1.08	4.50	0.131	6.281 ± 0.02	318.7 ± 1.1
15	1.53	3.18	0.189	6.220 ± 0.03	315.8 ± 1.4
16	0.73	2.64	0.0614	6.177 ± 0.03	313.8 ± 1.4
17	0.06	3.54	0.185	6.125 ± 0.03	311.5 ± 1.3
18	0.66	5.35	0.355	6.126 ± 0.02	311.5 ± 1.1
Integrated age:					299.3 ± 0.3
93MO8	*Muscovite*		*Single grain*		
1	100	0.43	28.5	–	–
2	24.99	2.75	4.12	5.1654 ± 0.31	266.9 ± 15.5
3	26.58	2.48	2.82	5.1560 ± 0.61	266.5 ± 32.3
4	79.72	0.64	14.7	1.2160 ± 1.91	67.9 ± 104.5
5	13.6	5.12	2.25	5.2509 ± 0.22	271.0 ± 10.8
6	0.12	15.33	0.112	5.8919 ± 0.10	301.3 ± 4.9
7	–	25.87	0.0843	5.8881 ± 0.06	301.1 ± 3.1
8	–	10.43	0.000 017 1	5.8848 ± 0.13	302.9 ± 6.4
9	–	36.93	0.000 004 85	5.8653 ± 0.04	302.0 ± 1.9
Integrated age:					294.4 ± 2.0

Appendix A (*continued*)

Steps	Atmospheric contamination (%)	$\%^{39}Ar$	$^{37}Ar_{Ca}/^{39}Ar_K$	$^{40}Ar^*/^{39}Ar_K$	Age $\pm 1\sigma$ (Ma)
93MO10	*Amphibole*		*Single grain*		
1	95.69	0.80	40.000	8.8995 ± 2.15	248.1 ± 55.9
2	60.92	0.51	9.870	8.7485 ± 1.25	244.1 ± 34.2
3	14.08	6.31	8.550	10.9437 ± 0.11	300.5 ± 2.8
4	4.17	23.90	6.630	11.0149 ± 0.05	302.3 ± 1.2
5	2.19	24.55	5.530	11.0064 ± 0.04	302.1 ± 0.9
6	1.96	8.36	5.190	10.9695 ± 0.09	301.2 ± 2.1
7	1.78	10.95	5.230	11.0841 ± 0.06	304.1 ± 1.6
8	2.89	4.63	6.490	10.1024 ± 0.12	304.5 ± 3.2
9	2.13	19.99	6.090	10.9902 ± 0.05	301.7 ± 1.2
Integrated age:					301.52 ± 0.72
93MO5	*Muscovite*		*Single grain*		
1	79.77	0.25	–	1.4401 ± 3.40	79.6 ± 1183.8
2	18.15	0.60	–	5.0901 ± 1.18	266.9 ± 57.5
3	7.66	0.77	–	5.6700 ± 1.14	295.0 ± 54.8
4	–	1.46	–	5.9883 ± 0.56	310.2 ± 26.8
5	0.66	19.5	0.005 60	5.8428 ± 0.05	303.3 ± 2.3
6	0.76	25.74	0.004 31	5.8174 ± 0.03	302.1 ± 1.6
7	1.99	11.42	0.011 195	5.7458 ± 0.08	298.7 ± 3.8
8	0.71	40.23	0.006 64	5.8360 ± 0.03	302.9 ± 1.3
Integrated age:					301.6 ± 1.2
95MO12A	*Muscovite*		*Single grain*		
1	31.16	1.85	0.0354	11.209 ± 0.38	306.6 ± 9.7
2	19.77	0.09	0.944	9.881 ± 5.18	272.9 ± 132.8
3	12.18	1.88	0.0369	11.270 ± 0.35	308.2 ± 8.9
4	9.33	1.31	0.000 006 41	10.505 ± 0.42	288.8 ± 10.7
5	10.78	2.68	0.000 003 14	10.862 ± 0.18	297.9 ± 4.6
6	2.02	33.13	0.003 57	10.963 ± 0.03	300.4 ± 0.6
7	0.79	33.67	0.000 000 250	11.035 ± 0.02	302.3 ± 0.6
8	0.60	25.38	0.000 000 332	11.037 ± 0.04	302.3 ± 0.9
Integrated age:					301.5 ± 0.5
93MO16	*Biotite*		*Single grain*		
1	8.45	5.03	0.001 93	5.5747 ± 0.07	290.5 ± 3.6
2	1.64	18.06	0.001 40	5.7891 ± 0.03	300.7 ± 1.4
3	1.31	9.42	0.002 48	5.7989 ± 0.03	301.2 ± 1.7
4	–	9.17	–	5.8706 ± 0.03	304.6 ± 1.9
5	–	5.16	0.000 47	5.8883 ± 0.07	305.5 ± 3.4
6	0.82	11.00	0.001 61	5.8110 ± 0.03	301.8 ± 1.6
7	0.72	18.68	0.001 68	5.8138 ± 0.02	301.9 ± 1.1
8	1.08	10.28	0.001 48	5.8147 ± 0.05	301.9 ± 2.4
9	–	6.9	0.003 60	5.8712 ± 0.05	304.7 ± 2.4
10	0.89	6.28	0.002 55	5.8326 ± 0.05	302.8 ± 2.6
Integrated age:					301.7 ± 0.6

Appendix A (*continued*)

Steps	Atmospheric contamination (%)	$\%^{39}Ar$	$^{37}Ar_{Ca}/^{39}Ar_K$	$^{40}Ar^*/^{39}Ar_K$	Age $\pm 1\sigma$ (Ma)
93MO16	*Muscovite*		*Single grain*		
1	100.0	–	–	–	–
2	1.35	2.65	0.000 011 6	5.466 ± 0.08	278.6 ± 3.8
3	3.98	1.65	0.000 018 7	5.226 ± 0.19	267.2 ± 9.1
4	0.02	2.33	0.0331	5.647 ± 0.13	287.1 ± 6.2
5	–	2.32	0.0404	5.777 ± 0.13	293.2 ± 6.1
6	–	1.02	0.000 030 2	5.440 ± 0.26	277.4 ± 12.2
7	0.96	2.01	0.0140	5.322 ± 0.17	271.8 ± 8.2
8	–	3.26	0.000 095 9	5.677 ± 0.10	288.5 ± 4.7
9	0.45	8.57	0.000 003 67	5.901 ± 0.04	299.0 ± 2.1
10	0.49	76.20	0.197	5.816 ± 0.01	295.0 ± 0.5
Integrated age:					293.4 ± 0.6
93MO11	*Biotite*		*Single grain*		
1	100	0.16	0.0000	–	–
2	12.29	4.11	0.0311	4.6039 ± 0.75	242.6 ± 36.9
3	5.23	7.46	0.0195	5.5707 ± 0.24	289.6 ± 11.6
4	–	19.12	0.0000	5.9072 ± 0.11	305.6 ± 5.5
5	–	22.31	0.0009	5.9041 ± 0.09	305.5 ± 4.3
6	0.03	29.31	0.0082	5.9138 ± 0.06	306.0 ± 2.9
7	4.84	5.23	0.0439	5.6183 ± 0.39	291.9 ± 18.9
8	4.88	2.73	0.0147	5.6776 ± 0.69	294.7 ± 33.1
9	2.53	9.56	0.0811	5.7722 ± 0.19	299.3 ± 9.2
Integrated age:					300.5 ± 2.9
95MO11	*Muscovite*		*Single grain*		
1	35.63	0.2	0.291	7.934 ± 2.25	222.3 ± 59.3
2	4.17	3.48	0.0240	11.349 ± 0.15	310.2 ± 3.7
3	–	2.61	0.000 003 05	11.622 ± 0.23	317.0 ± 5.6
4	–	2.40	0.000 003 31	11.298 ± 0.24	308.9 ± 6.0
5	1.50	3.42	0.0392	11.021 ± 0.17	301.9 ± 4.2
6	0.60	20.81	0.003 08	10.927 ± 0.03	299.5 ± 0.7
7	0.22	14.91	0.000 000 534	10.962 ± 0.05	300.4 ± 1.3
8	0.32	44.11	0.005 08	10.903 ± 0.03	298.9 ± 0.6
9	0.60	7.98	0.0226	10.943 ± 0.09	299.9 ± 2.3
Integrated age:					300.4 ± 0.5
95MO11	*Biotite*		*Single grain*		
1	38.45	1.99	0.0234	7.983 ± 0.09	223.6 ± 2.4
2	4.59	6.69	0.004 68	10.032 ± 0.03	276.8 ± 0.6
3	1.46	9.29	0.002 81	10.754 ± 0.03	295.2 ± 0.6
4	0.78	14.91	0.003 29	10.896 ± 0.02	298.8 ± 0.5
5	0.67	11.61	0.003 42	10.946 ± 0.02	300.0 ± 0.6
6	0.52	13.71	0.003 00	10.976 ± 0.02	300.8 ± 0.5
7	0.48	8.68	0.004 00	10.969 ± 0.02	300.6 ± 0.5
8	0.74	5.97	0.005 45	10.931 ± 0.02	299.6 ± 0.6
9	1.26	3.76	0.004 21	10.913 ± 0.04	299.2 ± 1.1
10	1.05	7.25	0.005 76	10.940 ± 0.02	299.9 ± 0.6
11	1.07	6.55	0.0127	10.927 ± 0.02	299.5 ± 0.5
12	0.57	9.60	0.0277	10.960 ± 0.02	300.4 ± 0.5
Integrated age:					296.4 ± 0.2

References

Amenzou, M., 1988. Les granitoïdes hercyniens du massif des Maures (Var, France). Etude géologique et minéralogique. Implications génétiques. Thèse doctorat, Nice, 280 pp.

Basso, A.M., 1985. Le Carbonifère de Basse Provence (SE de la France), évolution sédimentaire et structurale. 3rd cycle Thesis, Univ. Univ. Aix Marseille., 319 pp.

Bordet, P., 1966. Sur la structure du NW du Massif des Maures. C. R. Acad. Sci. 262, 2677–2680.

Boriani, A.C., Villa, I.M., 1997. Geochronology of regional metamorphism in the Ivrea–Verbano Zone and Serie dei Laghi, Italian Alps. Schweiz Mineral Petrogr. Mitt. 77 (3), 381–401.

Bouchot, V., Alexandrov, P., Monié, P., Morillon, A.-C., Cheilletz, A., Ruffet, G., Roig, J.-Y., Charonnat, X., Chauvet, A., Faure, M., Le Carlier, Ch., Cuney, M., Gama, S., Ramboz, C., Becq-Giraudon, J.-F., Truffert, C., Ledru, P., Milési, J.P., 1999. The W–As–Au–Sb metalliferous peak: an instantaneous marker of the late-orogenic evolution of the Variscan belt at 310–305 Ma. In: Document BRGM 293, Colloque Geofrance 3D, 33–35.

Bouloton, J., Goncalves, P., Pin, C., 1998. The La Croix-Valmer garnet-spinel peridotite (Central Maures): A cumulate of oceanic affinity involved in Early Variscan subduction. C. R. Acad. Sci. Ser. IIA, 326 (7), 473–477.

Burg, J.P., Brun, J.P., Van den Driessche, J., 1990. Le sillon houiller du massif central français: faille de transfert pendant l'amincissement crustal de la chaîne varisque? C. R. Acad. Sci. 311, 147–152.

Burg, J.P., Van den driessche, J., Brun, J.P., 1994. Syn- to post-thickening extension in the Variscan Belt of Western Europe: mode and structural consequences. Géologie de la France 3, 33–51.

Caen-Vachette, M., Couturié, J.P., Didier, J., 1982. Ages radiométriques des granites anatectitiques et tardi-magmatiques du Velay (Massif central français). C. R. Acad. Sci. 294, 135–138.

Caruba, C., 1983. Nouvelles données pétrographiques, minéralogiques et géochmiques sur le massif métamorphique hercynien des Maures (Var, France): comparaison avec les segments varisques voisins et essais d'interprétation géotectonique. Thèse doctorat, Nice.

Costa, S., 1990. De la collision continentale à l'extension tardi-orogénique: 100 Ma d'histoire varisque dans le Massif Central français, Thesis, Univ. Sciences et Techniques Montpellier, France.

Costa, S., Rey, P., 1995. Lower crustal rejuvenation and growth during post-thickening collapse: insights from a crustal cross section through a Variscan metamorphic core complex. Geology 23, 905–908.

Costa, S., Maluski, H., Lardeaux, J.M., 1993. Chronology of Variscan tectono-metamorphic events in an exhumed crustal nappe: the Monts du Lyonnais complex (Massif Central, France). Chem. Geol. (Isot. Geosci. Sect.) 105, 339–359.

Crevola, G., Pupin, J.-P., Toutin-Morin, N., 1991. La Provence varisque: structure et évolution géologique anté-triasique. Sci. Géol. Bull. 44, 287–310.

Downes, H., Kempton, P.D., Briot, D., Harmon Leyreloup, A., 1991. Pb and O isotope systematics in granulite facies xenoliths, French Massif Central: implication for crustal processes. Earth and Planetary Sciences Letters 102, 342–357.

Faure, J.F., 1995. Late orogenic Carboniferous extensions in the Variscan French Massif Central. Tectonics 14, 132–153.

Féraud, G., Gastaud, J., Auzende, J.M., Olivet, J.L., Cornen, G., 1982. ^{40}Ar–^{39}Ar ages for the alkaline volcanism and the basement of Gorringe Bank, North Atlantic Ocean. Earth Planet. Sci. Lett. 57, 211–226.

Gardien, V., Lardeaux, J.M., Ledru, P., Allemeand, P., Guillot, S., 1997. Metamorphism during the late orogenic extension: insights from the French Variscan Belt. Bull. Soc. Géol. Fr. 168 (3), 271–286.

Innocent, C., 1993. Contribution des isotopes à longue période à la reconnaissance de l'altération de la croûte continentale. Thesis, Aix-Marseille.

Le Marrec, A., 1976. Reconnaissance pétrographique et structurale des formations cristallophylliennes catazonales du Massif de Sainte-Maxime (quart NE du massif varisque des Maures, Var, France). Thesis, Aix-Marseille III.

Leyreloup, A., Buscail, F., Motard, C., Ciancaléoni, L., Dumoulin-Thiault, C., Lavigne, J.F., Monié, P., Brunel, M., 1996. Découvertes de paragenèse de types schistes blancs dans les Maures occidentales. Chemins *P–T–t*. Implications géodynamiques. Réunion Annuelle des Sciences de la Terre Conférence, Orléans, France.

Maluski, H., Allègre, C.J., 1970. Problème de la datation par le couple $^{87}Rb/^{87}Sr$ des socles gneissiques: exemple des gneiss de Bormes (massif hercynien des Maures, France). C. R. Acad. Sci. Paris 270, 18–21.

Maluski, H., 1972. Etude 87Rb/87Sr du massif granitique de Plan-de-la-Tour (Maures). C. R. Acad. Sci. Paris 274, 520–523.

Maluski, H., Gueirard, S., 1978. Mise en évidence par la méthode $^{40}Ar/^{39}Ar$ de l'âge à 580 Ma du granite de Barral (Massif des Maures, Var, France). C. R. Acad. Sci. Paris 287, 195–198.

Maquil, R., 1976. Contribution à l'étude pétrographique et structurale de la région Sud-Est du Massif des Maures. Annales de la Société Géologique de Belgique 99, 601–613.

Matte, P., 1991. Accretionary history and crustal evolution of the Variscan belt in Western Europe. Tectonophysics 196, 309–337.

Morillon, A.-C., 1997. Etude thermo-chronométrique appliquée aux exhumations et contexte orogénique: le Massif des Maures (France) et Les Cordillères Bétiques (Espagne). Thesis, Nice, 289 pp.

Moussavou, M., 1998. Contribution à l'histoire thermo-tectonique Varisque du Massif des Maures, par la typologie du zircon et la géochronologie U/Pb sur minéraux accessoires. Thesis, Montpellier, 179 pp.

Moussavou, M., Lancelot, J., 1996. Géochronologie Ur/Pb sur

zircons et monazites du Massif des Maures. Réunion Annuelle Sciences de la Terre Conférence, Orléans, France.
Onezime, J., Faure, M., Crevola, G., 1999. Petro-structural analysis of the Rouet–Plan-de-la-Tour granitic complex (Maures and Tanneron massifs, Var, France). C. R. Acad Sci. Ser. IiA 328 (11), 773–779.
Platt, J.P., 1993. Exhumation of high pressure rocks: a review of concepts and processes. Terra Nova 5, 119–133.
Rollet, N., 1999. Structures profondes et dynamique du bassin ligure et de ses marges, Thesis Univ. Paris VI, 292 pp.
Roubault, M.P., Bordet, F.L., Sonet, J., Zimmermann, J.L., 1970. Ages absolus des formations cristallophylliennes des Massifs des Maures et du Tanneron. C. R. Acad. Sci. Paris 271, 1067–1070.
Ruffet, G., Féraud, G., Amouric, M., 1991. Comparison of ^{40}Ar–^{39}Ar conventional and laser dating of biotites from the North Tregor Batholith. Geochem. Cosmoch. Acta 55, 1675–1688.
Steiger, R.H., Jäger, E., 1977. Submission on geochronology: convention in the use of decay constants in geo and cosmochronology. Earth Planet. Sci. Lett. 36, 359–362.
Toutin-Morin, N., Delfaud, J., Marocco, R., 1988. Dynamique des bassins permiens du Sud-Est de la France. Sédimentation, volcanisme, tectonique. Géologie Alpine Mém. Hs. 14, 29–38.
Turner, G., Huneke, J.C., Podosek, F.A., Wasserburg, G.J., 1971. ^{40}Ar–^{39}Ar ages and cosmic ray exposure ages of Apollo 14 samples. Earth Planet. Sci. Lett. 12, 19–35.
Vauchez, A., Bufalo, M., 1985. La limite Maures occidentales-Maures orientales (Var, France): un décrochement majeur entre deux provinces structurales très contrastées. C. R. Acad. Sci. Paris Sér. II 301 (14), 1059–1062.
Vauchez, A., Bufalo, M., 1988. Charriage crustal, anatexie, et décrochements ductiles dans les Maures orientales (Var, France) au cours de l'orogenèse varisque. Geol. Rundschau 77, 45–62.
Villa, I.M., 1998. Isotopic closure. Terra Nova 10, 42–57.
Zheng, J.S., Mermet, J.F., Toutin-Morin, N., Hanes, J., Gondolo, R., Morin, R., Féraud, G., 1992. Datation $^{40}Ar/^{39}Ar$ du magmatisme et de filons minéralisés permiens en Provence Orientale (France). Geodinamica Acta 5 (3), 203–215.